Nanoscale

Accepted Manuscript

This article can be cited before page numbers have been issued, to do this please use: Y. B. Seven, E. Seven, K. Parikh, M. Aydin, E. K. Luca, J. Nair, E. C. Kirbas and R. M. Leblanc, *Nanoscale*, 2025, DOI: 10.1039/D5NR02670A.

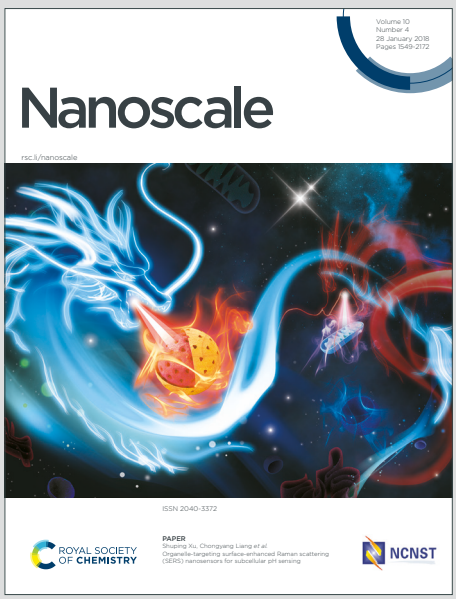

ROYAL SOCIETY OF CHEMISTRY

rsc.li/nanoscale

View Article Online
DOI: 10.1039/D5NR02670A

ARTICLE

Rapid mapping of spinal and supraspinal connectome via self-targeting glucose-based carbon dots

Received 00th January 20xx,
Accepted 00th January 20xx

DOI: 10.1039/x0xx00000x

Yasin B. Seven,*[a,b] Elif S. Seven,[c,d] Emel Kirbas Cilingir,[c] Komal Parikh,[e] Mehmet Aydin,[a] Edward K. Luca,[e] Jayakrishnan Nair,[f] and Roger M. Leblanc[c]

The spinal cord is a highly dynamic network playing significant roles in vital functions of the brain. Disorders of the spinal cord, such as spinal cord injury and amyotrophic lateral sclerosis (ALS), are associated with neurodegeneration, often resulting in morbidity and mortality. The blood-brain barrier (BBB) represents a major challenge against imaging and therapeutic agents as less than 2% of small-molecule drugs and almost no large-molecule drugs can cross the BBB. Furthermore, spatial spectroscopy studies show highly heterogeneous BBB crossing with significant accumulation at the unintended brain regions. Thus, targeting systems that can cross the BBB at the spinal cord and precisely target specific cell types/populations are vitally needed. Carbon dots can be custom-designed to accumulate at the spinal cord; thus, they offer great potential as delivery platforms for imaging and therapeutic approaches. Since neurons are metabolically highly active and rely on glucose, we designed glucose-based carbon dots (GluCDs) with ~4 nm in diameter and glucose-like surface groups. Thus, we determined the CNS distribution of GluCDs in three scales: 1. brain regional distribution, 2. cellular tropism (e.g. neurons *vs* glia), and 3. intracellular localization. We found that GluCDs: 1) cross the BBB at the spinal cord level, localize primarily to the spinal cord, and are quickly transported to higher centers in the brain, revealing supraspinal connectome within 4 hours after systemic delivery (minimally invasive and significantly faster than available technologies); 2) almost exclusively localize to neurons without the need for targeting ligand (neuronal self-targeting), 3) are confined to late endosomal/lysosomal compartment in neurons. Then, we verified our findings in a cervical spinal cord contusion injury model with GluCDs targeting neurons at the injury epicenter. Therefore, GluCDs can be used as robust imaging agents to take rapid snapshots of the spinal/supraspinal network. GluCDs nanoconjugates can open new avenues for targeted imaging of spinal cord injury. These findings can be extended to other spinal disorders such as ALS, spinal muscular atrophy, and spinal stroke.

Introduction

Delivery of imaging and therapeutic agents across the blood-brain barrier (BBB) is a formidable problem, limiting the development of effective neuroimaging and neurotherapeutic agents.[1-3] BBB represents a major obstacle as less than 2% of small-molecule drugs and almost no large-molecule drugs can cross the BBB.[4,5] Even the "BBB crossing" small molecules achieve much lower concentrations than the plasma.[6,7] Furthermore, according to spatial spectroscopy studies, these molecules show highly heterogeneous BBB crossing with significant targeting at the unintended brain regions or cell types/populations.[7] Thus, delivery systems that can cross the BBB at the desired brain regions and precisely target specific cell populations are vitally needed.

The spinal cord plays a significant role in the communication, data processing, and coordination between the brain and peripheral nervous system. Motor functions, such as breathing and locomotion, and sensory functions, such as pain and touch, rely on adequately functioning spinal circuits.[8-12] Spinal cord disorders such as spinal cord injury (SCI), spinal stroke in aortic surgery, amyotrophic lateral sclerosis (ALS), spinal muscular atrophy (SMA), Friedreich's ataxia, and multiple sclerosis are often associated with neuronal loss and highly dynamic reorganization of spinal and supraspinal networks.[13-16] Despite the prevalence and severity of these conditions, *there is no rapid and minimally invasive small molecule delivery system selectively targeting the spinal neurons and associated circuits*.

Carbon dots are spherical carbon-based nanoparticles with tunable physicochemical and optical properties.[17-19] Precursors and synthetic methods significantly affect the carbon dot properties and their interactions with the biological environment,[20] leading to differences in tissue distribution and biological interactions. Thus, carbon dots are highly customizable nanoplatforms, which can be conjugated with fluorophores, small molecule drugs, and siRNAs for imaging and therapeutic purposes.[21-23] Neurons are metabolically very active; relying primarily on glucose as their energy source. To

[a] Dept. of Physiological Sciences, University of Florida, Gainesville, FL, 32603, USA
[b] McKnight Brain Institute, University of Florida, Gainesville, FL, 32610, USA
[c] Department of Chemistry, University of Miami, Coral Gables, FL, 33146, USA
[d] C-Dots Nanotec LLC, Gainesville, FL, 32601, USA
[e] Dept. of Physical Therapy, University of Florida, Gainesville, FL, 32603, USA
[f] Dept. of Physical Therapy, Thomas Jefferson University, PA, 19107, USA
* Corresponding author. E-mail: yasinbseven@ufl.edu

View Article Online
DOI: 10.1039/D5NR02670A

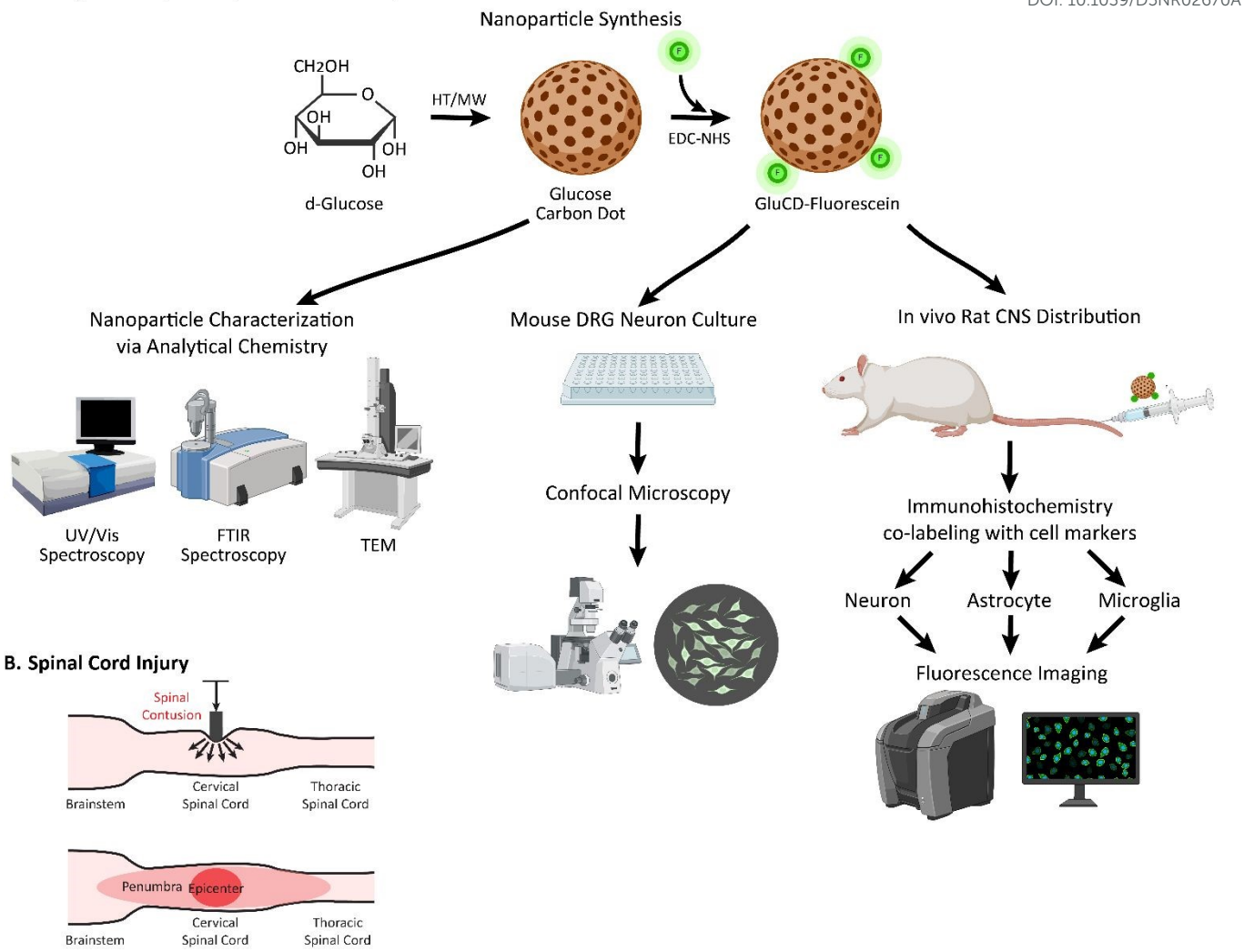

Fig. 1 Summary of methods: (A) Flowchart of the methods for GluCD characterization, *in vitro*, and *in vivo* studies. GluCDs were used for *in vitro* studies and GluCD-F was used for *in vivo* studies. Fluorescence imaging performed via epifluorescence and super-resolution confocal microscopies. (B) Spinal cord contusion was performed at the C4 level.

leverage neurons' high glucose demand to deliver imaging agents, we recently characterized ultrasmall, amphiphilic glucose-based carbon dots (GluCDs), which are ~4 nm in diameter, cross
the BBB *in vivo* and show no measurable cytotoxicity in healthy cell lines.[20,24,25] However, the distribution and the behavior of GluCDs in the central nervous system (CNS) are not yet described.

In this study, we determined the CNS distribution of GluCDs in three scales: 1. regional distribution (e.g. spinal cord, cerebellum, motor cortex, etc.), 2. cellular specificity/tropism (e.g. neurons, astrocytes), and 3. intracellular localization (cytoplasmic or a specific organelle). We showed that GluCDs 1. effectively cross the BBB selectively at the spinal cord level carrying small molecule cargo and quickly transported to higher centers in the brain *revealing spinal cord connectome faster than available technologies*, 2. almost exclusively localize to neurons without the need for targeting ligand, and 3. localize to late endosomes/lysosomes. In addition, we tested the GluCDs in a cervical SCI model and observed that GluCDs penetrate to injury epicenter and target neurons when administered intravenously after cervical SCI. Our findings indicate GluCDs nanoconjugates open new avenues for targeted imaging and treatment of SCI. These findings can be extended to other spinal disorders, such as ALS, SMA, and spinal stroke.

Results and Discussion

Glucose Carbon Dot Characterization

Following synthesis and purification, GluCDs were lyophilized to obtain a dry powder. The physical appearance of the GluCDs after lyophilization was brownish. GluCD yield was ~0.4% per initial d-glucose weight. To evaluate the utility of the GluCDs beyond initial synthesis, we next assessed their long-term stability. We observed comparable fluorescence intensities and central nervous system distribution of freshly prepared (Supp.

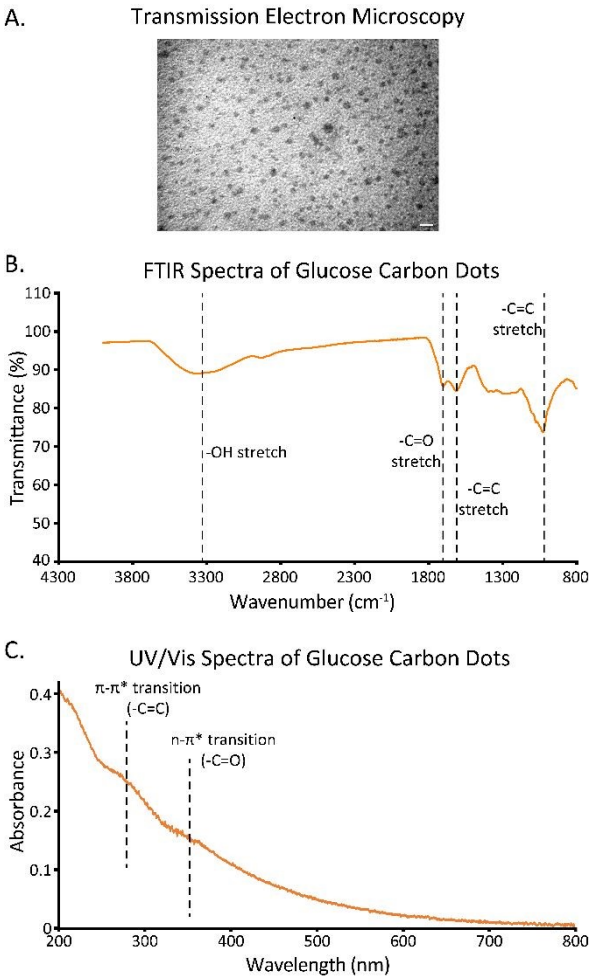

Fig.2 Characterization of glucose carbon dots: (A) Representative transmission electron microscopy image (Scale bar: 10 nm) (B) FTIR- (C) and UV/Vis spectra.

Fig.3) and 2-year-old batches[20], indicating strong stability. Furthermore, the photoluminescence intensity of GluCDs remained stable and did not quench after repeated imaging using fluorescence or confocal microscopy. PL of GluCDs is excitation-dependent, whereas the PL of GluCD-F is excitation independent (Supp Fig.3) consistent with our previous work.[25] We conducted additional characterization of CDs as a quality control measure to confirm batch-to-batch consistency of synthesis.[20,24,25]

Our earlier studies have characterized GluCDs and conjugates, extensively including UV/vis, PL, FTIR-ATR, XPS and Raman spectroscopy, TGA, TEM and AFM.[20,24,25] Fig. 2A shows a representative image from TEM showing round-shaped GluCDs. The diameters of GluCDs used in the studies are within the range of 3 to 8 nm.[20] GluCDs were covalently conjugated to fluorescein (GluCD-F), and characterized earlier[20,25] to test the cargo loading and enhance the fluorescence intensity.[20,24,25] Fourier-transform infrared (FTIR) spectrum of GluCDs is shown in Figure 2B. The wide prominent peak centered around 3335 cm^{-1} is consistent with hydroxyl groups (-OH stretch) in all samples. The sharp peak at 1020 cm^{-1} is mainly due to C-O stretching in C-O-C and C-O-H bonds. The peaks at 1703 nm and 1610 nm correspond to C=O and C=C bonds, respectively. UV/vis spectrum (Fig. 2C) shows two bands between 200 nm and 300 nm, suggesting π-π* transition likely due to aromatic ring formation.[20]

Glucose Carbon Dots Target Spinal Neurons with High Specificity and Localize to Late-Endosomal/Lysosomal Compartment

After GluCD-F administration via tail injections, initial observations suggested GluCD-F presence throughout the spinal cord, most likely due to the higher permeability of the BBB at the spinal cord level.[26-28] In contrast, only a few centers were targeted in the higher brain centers. In imaging studies, 45 minutes after intravenous delivery, the fluorescence intensity was minimal at the cervical spinal cord. However, four hours following delivery, significant green fluorescence was observed in the grey matter, which remained for at least 5 days (the longest time point verified).

Next, GluCD-F was co-immunolabelled with a neuronal marker (NeuN), astrocytic marker (GFAP), or microglial marker (IBA1) to study the cellular specificity. Fig. 3A and B show that GluCD-F is almost exclusively colocalized with NeuN+ neurons and distributed in a granular fashion in the perinuclear compartment of the cytoplasm. Thus, once internalized at the cell membrane, GluCDs are retrogradely carried to the perinuclear region. We quantified the ratio of fluorescein fluorescence in cell marker-labelled regions to the fluorescence in the entire image. Approximately 94.5% of the total fluorescence is observed within the NeuN+ areas, displaying strong neurotropism (Fig. 3C). NeuN labelled neuronal nuclei and cell bodies (somata). We observed that NeuN labels neuronal nuclei and somata, but not distal dendrites and axons, indicating that this number is conservative. Astrocytes did not detectably contain GluCDs, whereas microglia contained <5% of the GluCDs. To support the colocalization analyses, we performed a 2-dimensional Pearson's correlation coefficient between each cell marker with GluCDs (Fig. 3D). GluCD-treated astrocytes and microglia were indifferent than saline controls (0-15%). In contrast, neurons showed significant correlation with GluCD (~40%). GluCDs localize to nearly all neurons in the cervical spinal cord rather than a subset of them. Two observers counted 98.3% of NeuN+ neurons contained GluCD with a range of 95.9-100% per spinal cord section. Overall, GluCDs were effectively crossing the blood-spinal cord barrier and localize extensively to spinal neurons rather than glia (Fig. 3, Supplementary Fig. 1). Neuroimmune response is a major concern for viral targeting methods[29] and non-functionalized nanomaterials crossing the BBB as they are frequently scavenged by macrophages and microglia.[30-33] Hence nanomaterials escaping microglia are crucial to target other cell types in the CNS, such as neurons. Here, we leveraged neurons' high glucose demand to deliver GluCDs with glucose-like surface groups; suggesting self-targeting property.[25] Furthermore, microglia do not show proinflammatory phenotype suggesting favourable biocompatibility. Lastly, we generated rat dorsal root ganglion (DRG) cultures to confirm if GluCDs have the ability to target neurons outside the BBB. Fig 3E shows that rat DRG neurons are positive for GluCDs.

To determine the intracellular localization, we performed LAMP1 immunohistochemistry. LAMP1 is a late endosomal and lysosomal marker. Fig. 4 shows nearly complete overlap between GluCDs and LAMP1, suggesting that GluCDs localize to late endosomes and lysosomes. Of particular note, GluCDs are distributed homogeneously in the perinuclear compartment with some polarized clustering of lysosomes (Fig. 4A-B,

View Article Online
DOI: 10.1039/D5NR02670A

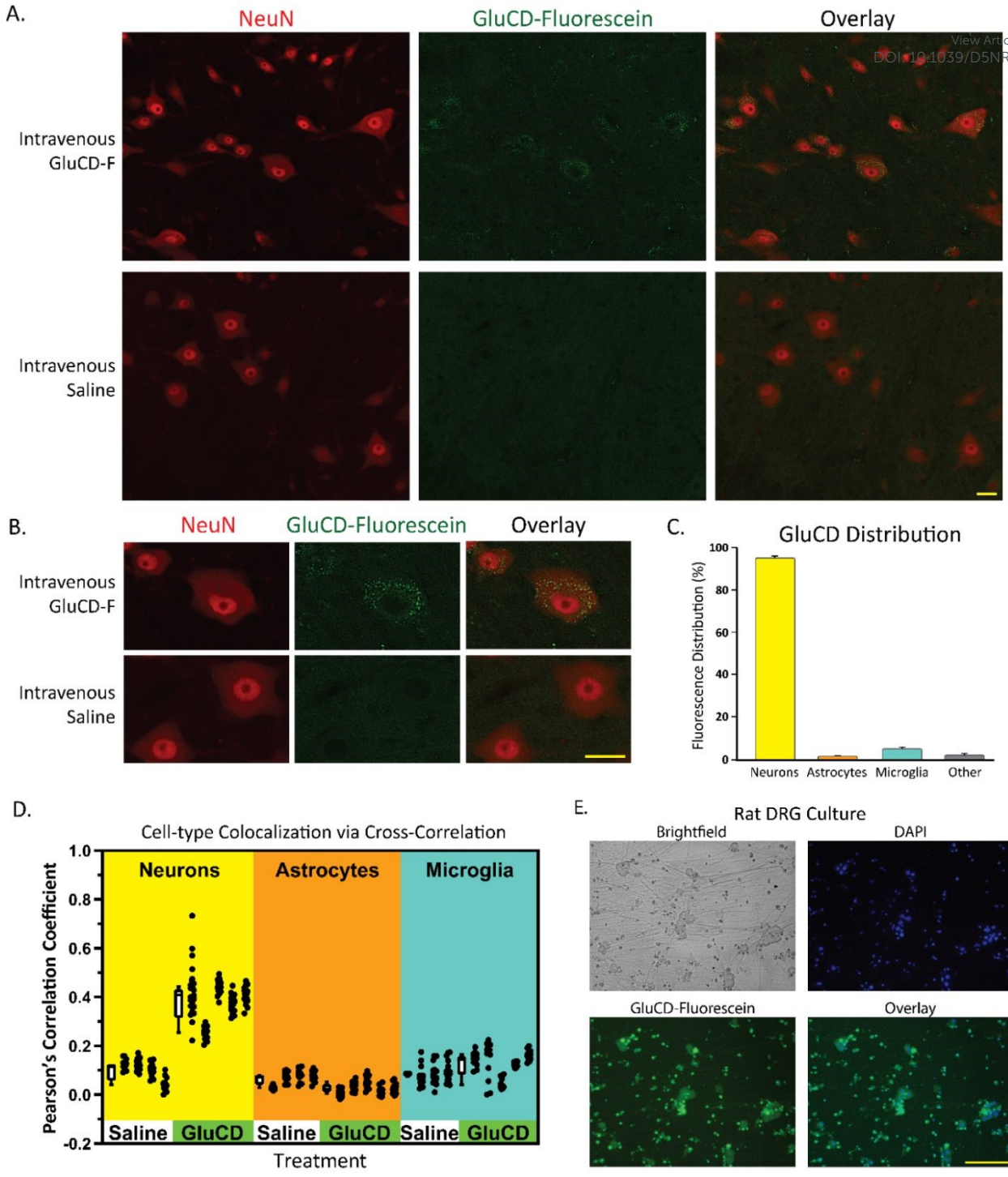

Fig.3 Neuronal colocalization of glucose carbon dot-fluorescein (GluCD-F) conjugates in the cervical spinal cord following intravenous delivery. (A) Representative histological sections following GluCD-F (top panels) or saline (bottom panels) administration. In the left panels, neurons are labelled with NeuN (red). Middle panels show GluCD-F localization (green). The right panels show the colocalization via the overlay. GluCD-F colocalize with neurons. Scale bar: 25 µm (B) Zoomed-in view showing the neuronal colocalization and the granular distribution of GluCD-F. Scale bar: 25 µm (C) Approximately 95% of all fluorescence colocalize with neurons. ~4% colocalize with microglia. (D) Pearson's cross-correlation coefficients between red and green channels are shown by image to determine the distribution by cell types. The of GluCD-F correlates with neuronal marker, but not others. (E) Histological visualization of GluCD-F treatment in rat DRG neuron cultures. The first figure is a brightfield overview. Nuclei are shown by DAPI (blue). Green fluorescence shows the GluCD-F uptake. Scale bar: 100 µm

Supplementary Fig. 2). Finally, we also confirmed the intracellular GluCD distribution via 3D super-resolution confocal microscopy (Supplementary video). These results suggest that GluCDs can be used for imaging of neuronal lysosomes, which can be invaluable for studying spatial lysosomal dynamics.

Glucose Carbon Dots Rapidly Reveal Supraspinal Connectome within 4 hours, Much Faster Than Previously Established Techniques

GluCD localization studies in the medulla, midbrain, cerebrum, and cerebellum showed that GluCD localization is not as extensive as in the spinal cord and does not follow a diffuse pattern when present. Often, GluCDs target a particular band or a focal area of neurons but not the adjacent centers. Furthermore, GluCDs are localized in neurons to specific brain centers, mostly with direct connections to the spinal cord. The primary areas of GluCD targeting were the area associated with premotor neurons in the medulla, thalamus, lamina/layer V at the cerebral cortex, and some olfactory areas such as the piriform cortex.[13] Fig. 5 shows the lamina V and thalamus labelling, which is not a diffuse pattern but a select group of cells. These connections are likely direct sensory or motor connections to the spinal cord. In addition, some neurons indirectly connected to the spinal cord, such as Purkinje neurons were also GluCD+, suggesting the possibility of GluCDs crossing the synapses to higher order neurons.

GluCD targeting occurs at most within 4 hours after intravenous administration and lasts up to 5 days (maximum time-span experiments were conducted). In comparison, retrograde labelling methods commonly used often take 2-14 days. Some examples of these traces are fluorogold (3-13 days[34-37]), fast blue (3-14 days[38-41]), cholera toxin beta subunit (2-3 days[42,43]), wheat germ agglutinin (2-3 days[44-47]), pseudo-rabies virus (24-48 hours[48-53]). More recent methods of AAV-mediated retrograde labelling are invasive and take 7-14 days. A recent elegant study of AAV-mediated supraspinal connectome tracing needed 2-4 weeks post-spinal injection.[13] We observed significant overlap in the brain regions labelled between intraspinal AAV injections of Wang et al. and our rapid

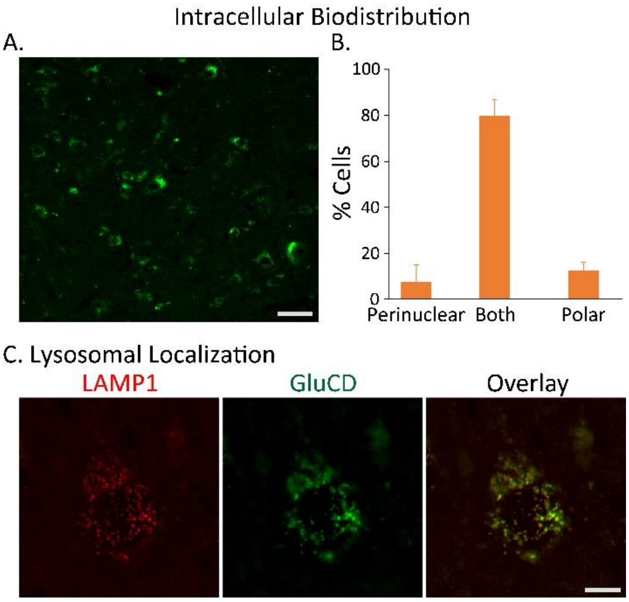

minimally invasive (intravenous) method. Thus, GluCD method offers a minimally invasive method, which provides a snapshot of supraspinal connectivity faster than the current methods. This method can be very useful to elucidate highly dynamic neural architecture of the spinal and supraspinal pathways in health and disease.[13]

Fig.4 Intracellular distribution of glucose-based carbon dots (GluCDs). (A) Cervical spinal distribution of GluCDs showing neuronal features. (B) Perinuclear symmetric distribution with polarization is the most common intracellular distribution. (C) GluCDs are colocalized with LAMP1-positive intracellular vesicles, i.e., late endosomes / lysosomes. Scale bars: 50 µm (A) and 10 µm (C).

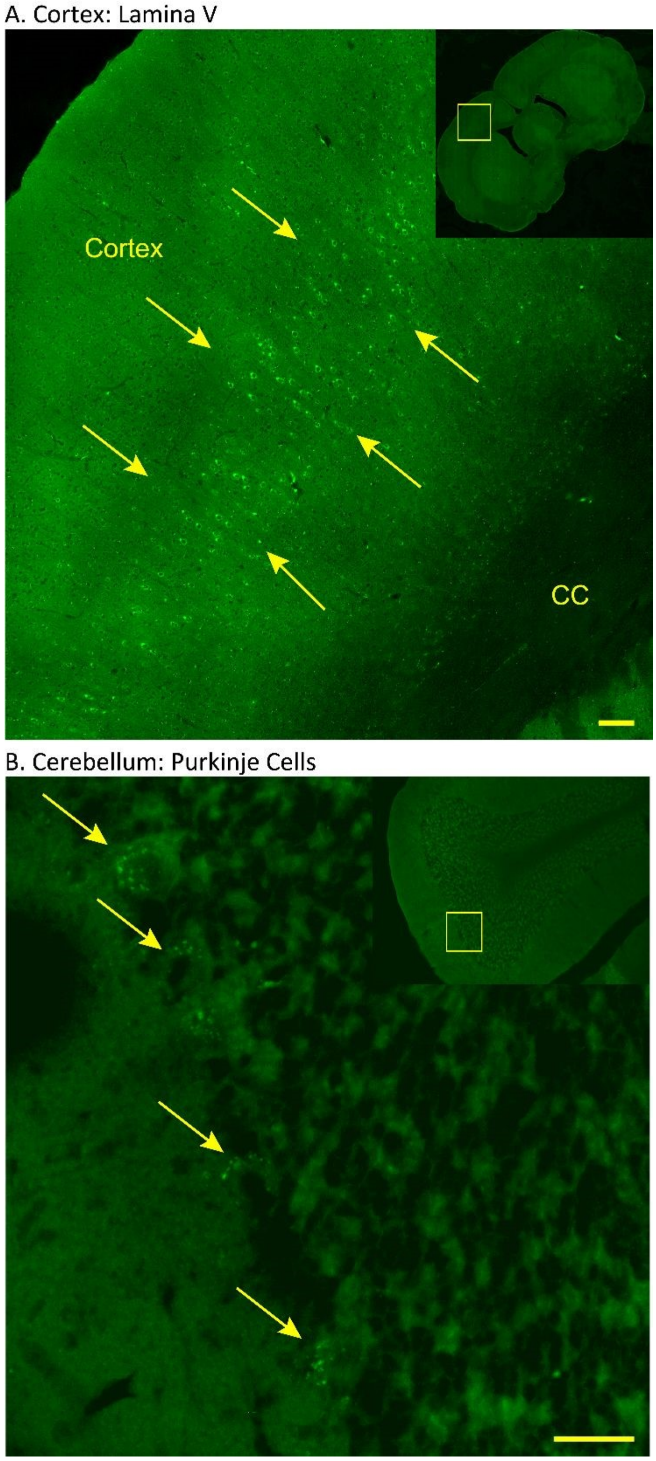

Fig.5 Representative images of glucose carbon dot targeting the supraspinal network. (A) Cortex: Layer V neurons are selectively positive for GluCD. Other layers are devoid of GluCDs (green). (B) Purkinje cells in the cerebellum are GluCD-positive. Scale bars: 100 µm (A) and 30 µm (C).

Glucose Carbon Dots Penetrate to Injury Epicenter and Maintain Neurotropism after Cervical Spinal Cord Contusion Injury

An important problem involving the spinal cord is the SCI. Cervical SCI is very commonly observed in vehicle accidents, where the blood supply to the spinal cord is impaired via acute hypotension and disruption to the local microvasculature, followed by coagulation. Thus, blood flow is the most impaired in the areas where therapeutics are needed the most. To determine the targeting efficacy of GluCDs to the epicenter of the SCI, we performed mid-cervical spinal contusion at C3/4 segment and waited 3 hours to administer GluCDs; much longer than expected for coagulation to take place. Four hours after administration, we determined the biodistribution of the GluCDs in the spinal cord. Similar to intact animals, GluCDs were present in neurons after injury (Fig. 6). Neuronal fluorescence intensities were stronger in the soma and dendrites at the injury epicenter, suggesting that neuronal GluCD uptake is enhanced with acute SCI.

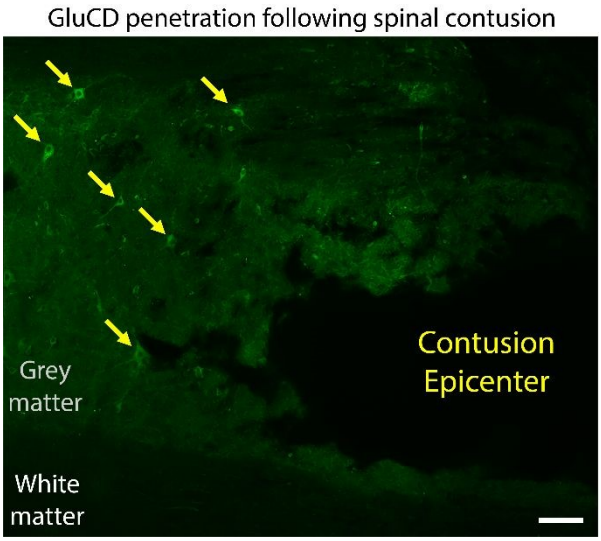

Fig.6 Representative image of a longitudinal section of cervical spinal cord with glucose carbon dot (GluCD) treatment after mid-cervical spinal contusion injury. Neuronal somata (grey matter) are GluCD-positive. Scale bar = 200 µm

Conclusion

The BBB and innate immune responses are major obstacles in the delivery of imaging agents and therapeutics for various neurological disorders. Therefore, it is crucial to develop minimally invasive and less immunogenic delivery platforms that can effectively and robustly cross the BBB and reach the CNS. Here, we are reporting glucose-based carbon dots, which can cross the BBB selectively in the spinal cord likely due to increased permeability of the BBB at the spinal cord [26-28] (Figure 7A & B). Furthermore, GluCDs localize to spinal neurons with high specificity (Figure 7). Then, GluCDs retrogradely target the supraspinal network following the spinal route (Figure 7B); more rapidly than currently available techniques. Intracellularly, neuronal lysosomes appear to be the target organelle (Figure 7C). Importantly, GluCDs effectively penetrated into the spinal contusion injury epicenter. Thus, GluCDs may be effective imaging and therapeutic delivery tools for the neurological disorders of spinal cord.

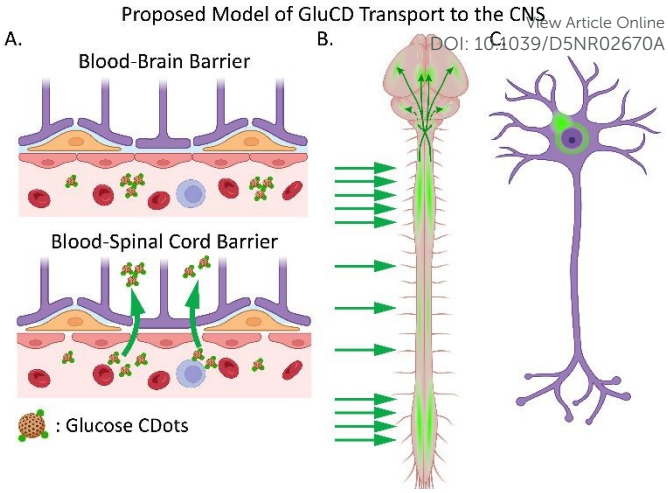

Fig.7 Proposed model of glucose carbon dot (GluCD) transport to the central nervous system (CNS). (A) GluCDs cross the CNS barrier at the spinal cord level. (B) GluCDs are carried to higher centers targeting supraspinal connectome. (C) GluCDs are neurotropic with late endosomal/lysosomal localization.

Experimental

Materials and Instrumentation

D-glucose and NaOH pellets (98.5 %) (nitrogen flushed, hygroscopic) were purchased from VWR International, LLC (Radnor, PA) and Acros Organics, respectively. DI-H_2O with a resistivity of 18 MΩ·cm at 20.0 ± 0.5°C and surface tension of 71.2 mN·m^{-1} was used for all reactions and purification steps (Direct-Q 3 water purification system; EMD Millipore Corp.; Chicago, IL). Pre-treated Spectra/Por 7 dialysis membrane tubing (1 kDa MWCO, Spectrum Laboratories Supply, Inc., Rancho Dominguez, CA) and syringe filters (0.2 µm, VWR, Radnor, PA) were used for GluCD purification. The samples were lyophilized using a FreeZone 4.5 L cascade benchtop freeze dry system (Labconco, Kansas City, MO). All aqueous CD samples were sonicated prior to characterization using a Branson 1510 ultrasonicator (Gaithersburg, MD). All chemicals were used as received without further purification.

Carbon Dot Preparation

GluCDs are prepared using a bottom-up approach with glucose as the sole precursor via our previously published hydrothermal carbonization method.[20,24,25] Hydrothermal carbonization was performed in a Teflon-coated autoclave reactor with glucose dissolved in ultrapure water at a final concentration of 10% w/w. The reaction temperature was set to 200°C for a duration of 5 h. After the reaction, everything in the reactor was transferred to a centrifuge tube and centrifuged at 3000 rpm, at 4°C for 20 min. The supernatant was syringe-filtered to get rid of all the leftover precipitation. The filtered solution was neutralized using a super-saturated NaOH solution. Finally, the sample was lyophilized to yield a solid product. GluCD-F

conjugates were prepared with EDC-NHS ester conjugation using our previously published medhod.[25]

Characterization of Carbon Dots

UV/vis absorption spectra of CDs dispersed in DI-H_2O were acquired using a Cary 100 UV/vis spectrophotometer (Agilent Technologies, Inc.; Santa Clara, CA, USA) and a semi-micro-quartz cuvette with 1 cm pathlength and two dark walls (Starna Cells, Inc). Photoluminescence (PL) emission spectra were obtained employing a Horiba Jobin Yvon Fluorolog-3 (Horiba, Ltd.; Piscataway, NJ, USA) with a slit width of 5 nm for both excitation and emission. A quartz cuvette with all clear walls and a 1-cm pathlength (Starna Cells, Inc) was used for the PL emission measurements. Data analysis and plotting were done using ORIGIN Software (OriginLab Corp., Northampton, MA). Fourier-transform infrared spectroscopy equipped with attenuated total reflection accessories (FTIR-ATR, Perkin Elmer, Inc.; Waltham, MA, USA) was used to acquire FTIR spectra of lyophilized CDs with air as background.

A JEOL 1200x transmission electron microscope (TEM) was used for morphological studies using a carbon-coated copper grid. A drop of the aqueous CDs solution placed on the grid and air dried before imaging.

Rat Dorsal Root Ganglion Cultures

Rat dorsal root ganglion (DRG) neuron cultures for bioimaging studies were generously provided by Yelena Pressman at the University of Miami. DRG neurons were isolated from the dorsal root ganglia of embryonic rats (E15) according to an established protocol.[58] DRG neurons were plated on poly-L-lysine/laminin-coated 24-well (Corning, NY, US) plates in neurobasal media supplemented with B-27, L-glutamine and nerve growth factor (Gibco). Cultures were treated with 10 µM fluorodeoxyuridine to prevent contamination. First, to show viability of neurons in the culture immunocytochemistry was performed for neurofilament and β-Tubulin. One week after isolation, neurons were treated with 500 µM concentration of GluCD-Fluorescein for 24 hours, followed by PBS washes, and pre-fixed with a couple of drops of fresh 4% paraformaldehyde (PFA) for 5 minutes. PBS and PFA were aspirated gently, and neurons were post-fixed with fresh 4% PFA for 10 minutes, followed by PBS wash (2x). After fixation, we blocked the DRGs with 5% bovine serum albumin (BSA) with 0.6% Triton-X100. Primary antibodies targeting neurofilament (Thermo Fisher Scientific, Waltham, MA) and β-tubulin (Cell Signaling, Danvers, MA) were applied. For negative controls, neurons were incubated with antibody diluent only (2.5% BSA, 0.3% Triton-X100 in PBS). Secondary antibodies, Alexa Fluor 594 goat anti-mouse and Alexa Fluor 488 goat anti-rabbit (Thermo Fisher Scientific, Waltham, MA), were then applied. One drop of antifade reagent with DAPI was added and one cover slip was inserted carefully on top of each well before imaging with an EVOS Floid Cell Fluorescent Microscope.

Animals

Animal experiments were approved by the Institutional Animal Care and Use Committee at the University of Florida in accordance with the National Institutes of Health Guide and Use of Laboratory Animals. 19 adult male Sprague-Dawley rats were studied (~350-400 g, Harlan, Indianapolis IN, Colony 208A). Rats were maintained on a 12-h light/dark cycle with access to food and water ad libitum.

Intravenous Injections

Anesthesia was induced in a gas chamber (2.5% isoflurane in O2) and maintained via a nose cone (2% isoflurane in O2) on a surgical heating pad. Intravenous (IV) injections were performed at the lateral tail vein as described earlier.[55,56] Tail vein was catheterized (24 Gauge; Surflash, Somerset, NJ) and administered with GluCD-F conjugate in sterile saline (0.9% NaCl) or vehicle. The total dose of GluCD-F was 10 mg/kg at 2 mg/ml (mass/volume). Then, the intravenous catheter was removed, and the injection site was pressurized until bleeding stopped. Rats were kept awake for 45 min (imaging), 4 h (imaging) or 7 days (imaging and toxicity, Supp. Fig. 4). In addition to cellular toxicity analyses[20], no abnormal signs of stress were observed *in vivo*. Weight gains were normal for 7 days after GluCD delivery and microglia were not activated.

C4 Spinal Contusion

Anesthetic and surgical preparation methods have been previously described.[57-60] First, anesthesia was induced in a gas chamber (3% isoflurane in O_2) and maintained via a nose cone (2-2.5% isoflurane in O_2) during surgery. The adequacy of anesthesia was verified by the absence of toe pinch reflex. A heating pad was used to maintain the body temperature. Artificial tears were applied, and nails were clipped. Meloxicam (2 mg/kg) was administered subcutaneously to minimize inflammation. The surgical area was shaved and cleaned with betadine.

Following a cervical incision from the base of the skull to the C6 segment, C4 spinal cord was exposed via laminectomy while keeping the dura intact. A midline contusion was performed using the Infinite Horizons Impactor (Precision Systems and Instrumentation, LLC, Lexington, KY) after the spine was stabilized via 2 forceps near C3 and C5 levels.[61-64] A 1.3 mm-diameter tip was used to deliver 125 kdyn force with 0-s dwell time. Probe force and displacement were measured in real-time to ensure no accidental bone impacts occurred. Following contusion, muscles were sutured, and skin was closed with wound clips. Sterile lactated Ringer's solution (5mL) was administered subcutaneously for fluid loss due to surgery. Nanoconjugates were delivered IV 3 hours after injury. Rats were sacrificed at 7 h post-injury for further analyses.

Histology and Immunolabeling

All rats were perfused transcardially with 0.01 M PBS (4°C, pH 7.4) followed by 4% paraformaldehyde (PFA) in 0.01 M PBS (4°C, pH 7.4) at the terminal time points. Brain and spinal cord were harvested, fixed in 4% PFA (4°C, pH 7.4) overnight, and cryoprotected in 20% followed by 30% sucrose solution (4°C). Harvested tissues were protected from light as possible. All tissues were sectioned in the transverse plane using a freezing

View Article Online
DOI: 10.1039/D5NR02670A

microtome (40-µm thickness; SM2010R, Leica; Buffalo Grove, IL). Sectioned tissue slices were stored in antifreeze solution (30% glycerol + 30% ethylene glycol + 40% 0.1 M PBS) at −20°C. more than 6 cervical spinal samples and 8 medulla samples were uniformly selected for histological analyses.[60]

Immunohistochemistry was performed to label different cell types in the cervical spinal cord. Each cell marker protein was immunolabeled in a single batch to reduce batch-to-batch variability. Tissues were triple-washed in PBS (0.1M, pH 7.4) and incubated with 5% normal donkey serum (NDS), 0.1% bovine serum albumin, and 0.1% Triton X-100 in 0.1 M PBS (PBS-Tx) for 1 h. Then, tissues were incubated with one of the following: 1) mouse anti-NeuN (Neurons, 1:500; catalog no: MAB377, Millipore Sigma), 2) rabbit anti-GFAP (Astrocytes, 1:1000, catalog no: AB5804, Millipore), 3) mouse anti-IBA1 (Microglia, 1:500, catalog no: MABN92, Millipore), and 4) rabbit anti-LAMP1 (Late endosomes/lysosomes, 1:250, catalog no: 9091, Cell Signalling) primary antibodies in 2.5% NDS with PBS-Tx at 4ºC for 2 overnights. Tissues were triple-washed in PBS and incubated in donkey anti-mouse or donkey anti-rabbit (594, 1:500, Thermofisher) secondary antibodies, 2.5% NDS, and PBS-Tx at room temperature for 2 h. After the final wash, tissue sections were mounted on charged slides (Fisher) with hard-set anti-fade medium (Vector Labs) and cover-slipped. On a separate set of control tissues, no immunohistochemistry was performed to confirm if the nanoconjugate distribution in immunohistochemistry-treated and untreated tissues were the same.

Image Acquisition and Analysis

Tissue sections were imaged via epifluorescence and siper-resolution confocal microscopies. First, imaging was performed using an epifluorescence microscope with a 20x PlanApo lens (Keyence BZ-X700, Keyence Corporation of America, Itasca, IL). GluCD-Fluorescein conjugate was imaged at the excitation and emission wavelengths of 470/40 nm and 525/50 nm (GFP filter: OP-87763). Cell markers were imaged at the excitation and emission wavelengths of 560/40 nm and 630/75 nm (Texas red filter: OP-87765). For each image set (e.g., Neuronal marker + GluCD-Fluorescein), the image acquisition settings were used for both vehicle and treatment groups. We determined nanoconjugate colocalization using 3 methods: 1) %Colocalization: Determining the total nanoconjugate fluorescence intensity within a cell type divided by the overall total nanoconjugate fluorescence intensity, 2) Pixel-to-pixel 2-dimensional cross-correlation between nanoconjugate fluorescence intensity and cell marker intensity with MATLAB, and 3) Cell-by-cell classification of nanoconjugate positive/negative cells by 2 independent operators. We confirmed our intracellular localization and distribution findings using a Nikon CSU-W1 SoRa super-resolution confocal microscope (112x, 40x lens, 2.8x intermediate magnification, 488 nm). Furthermore, we quantified the symmetry of the intracellular distribution of the nanoparticles. Student's t-test was used to test the effects of nanoconjugate treatment compared to the vehicle group (SAS JMP Inc, Cary, NC). Differences were considered significant if $p<0.05$.

Author contributions

YBS: Conceptualization, funding acquisition, experimental design, performed experiments, analyzed data, provided supervision, wrote the first draft of manuscript, reviewed and edited the manuscript. ESS: Experimental design, performed experiments, analyzed data, wrote the first draft of manuscript, reviewed and edited the manuscript. EKC: Performed experiments, analyzed data, reviewed and edited the manuscript. KP: Performed experiments, analyzed data, reviewed and edited the manuscript. MA: Performed experiments, analyzed data, reviewed and edited the manuscript. EKL: Analyzed data, reviewed and edited the manuscript. JN: Analyzed data, reviewed and edited the manuscript. RML: Funding acquisition, provided supervision, reviewed and edited the manuscript.

Conflicts of interest

There are no conflicts to declare.

Data availability

Data is available upon request to the authors.

Acknowledgements

YBS is supported by NIH grant R21NS119862, Department of Physiological Sciences, McKnight Brain Institute, and TUBITAK grant 1059B142301280. RML is thankful for the grants from NSF (Grant numbers: 1809060 and 2041413) and from NIH (SUB00002778) to support this work. We would like to thank Adamantios Mamais for technical help with the super-resolution confocal imaging.

References

1. R. H. Muller and C. M. Keck, *J Biotechnol*, 2004, **113**, 151-170.
2. W. M. Pardridge, *J Cereb Blood Flow Metab*, 2012, **32**, 1959-1972.
3. M. M. Patel and B. M. Patel, *CNS Drugs*, 2017, **31**, 109-133.
4. W. M. Pardridge, *NeuroRx*, 2005, **2**, 3-14.
5. W. M. Pardridge, *Drug Discov Today*, 2007, **12**, 54-61.
6. H. Liu, K. Dong, W. Zhang, S. G. Summerfield and G. C. Terstappen, *Drug Discov Today*, 2018, **23**, 1357-1372.
7. D. Luptáková, T. Vallianatou, A. Nilsson, R. Shariatgorji, M. Hammarlund-Udenaes, I. Loryan and P. E. Andrén, *Mol Psychiatry*, 2021, **26**, 7732-7745.
8. C. E. Brown-Séquard, *Philadelphia University of California Libraries*, 1858.
9. F. W. Mott, *Proceedings of the Royal Society of London*, 1892, **50**, 120 - 121.
10. W. T. Porter, *J Physiol*, 1895, **17**, 455-485.
11. N. B. Finnerup and C. Baastrup, *Curr Pain Headache Rep*, 2012, **16**, 207-216.
12. A. D. Mickle, S. M. Won, K. N. Noh, J. Yoon, K. W. Meacham, Y. Xue, L. A. McIlvried, B. A. Copits, V. K. Samineni, K. E. Crawford, D. H. Kim, P. Srivastava, B. H. Kim, S. Min, Y. Shiuan, Y. Yun, M. A. Payne, J. Zhang, H. Jang, Y. Li, H. H. Lai, Y. Huang, S. I. Park, R. W. t. Gereau and J. A. Rogers, *Nature*, 2019, **565**, 361-365.
13. Z. Wang, A. Romanski, V. Mehra, Y. Wang, M. Brannigan, B. C. Campbell, G. A. Petsko, P. Tsoulfas and M. G. Blackmore, *Elife*, 2022, **11**.
14. A. C. Waddimba, N. B. Jain, K. Stolzmann, D. R. Gagnon, J. F. Burgess, Jr., L. E. Kazis and E. Garshick, *Arch Phys Med Rehabil*, 2009, **90**, 193-200.
15. M. E. van den Berg, J. M. Castellote, J. de Pedro-Cuesta and I. Mahillo-Fernandez, *J Neurotrauma*, 2010, **27**, 1517-1528.
16. M. J. Fishburn, R. J. Marino and J. F. Ditunno, Jr., *Arch Phys Med Rehabil*, 1990, **71**, 197-200.
17. J. E. Riggs, Z. Guo, D. L. Carroll and Y.-P. Sun, *Journal of the American Chemical Society*, 2000, **122**, 5879-5880.
18. Y.-P. Sun, B. Zhou, Y. Lin, W. Wang, K. A. S. Fernando, P. Pathak, M. J. Meziani, B. A. Harruff, X. Wang, H. Wang, P. G. Luo, H. Yang, M. E. Kose, B. Chen, L. M. Veca and S.-Y. Xie, *Journal of the American Chemical Society*, 2006, **128**, 7756-7757.
19. X. Xu, R. Ray, Y. Gu, H. J. Ploehn, L. Gearheart, K. Raker and W. A. Scrivens, *J Am Chem Soc*, 2004, **126**, 12736-12737.
20. E. S. Seven, E. Kirbas Cilingir, M. Bartoli, Y. Zhou, R. Sampson, W. Shi, Z. Peng, R. Ram Pandey, C. C. Chusuei, A. Tagliaferro, S. Vanni, R. M. Graham, Y. B. Seven and R. M. Leblanc, *J Colloid Interface Sci*, 2023, **630**, 306-321.
21. S. D. Hettiarachchi, R. M. Graham, K. J. Mintz, Y. Zhou, S. Vanni, Z. Peng and R. M. Leblanc, *Nanoscale*, 2019, **11**, 6192-6205.
22. S. D. Hettiarachchi, E. Kirbas Cilingir, H. Maklouf, E. S. Seven, S. Paudyal, S. Vanni, R. M. Graham and R. M. Leblanc, *Nanoscale*, 2021, **13**, 5507-5518.
23. P. Y. Liyanage, S. D. Hettiarachchi, Y. Zhou, A. Ouhtit, E. S. Seven, C. Y. Oztan, E. Celik and R. M. Leblanc, *Biochim Biophys Acta Rev Cancer*, 2019, **1871**, 419-433.
24. E. S. Seven, S. K. Sharma, D. Meziane, Y. Zhou, K. J. Mintz, R. R. Pandey, C. C. Chusuei and R. M. Leblanc, *Langmuir*, 2019, **35**, 6708-6718.
25. E. S. Seven, Y. B. Seven, Y. Zhou, S. Poudel-Sharma, J. J. Diaz-Rucco, E. Kirbas Cilingir, G. S. Mitchell, J. D. Van Dyken and R. M. Leblanc, *Nanoscale Adv*, 2021, **3**, 3942-3953.
26. W. A. Banks, A. J. Kastin and E. G. Gutierrez, *Neurosci Lett*, 1994, **179**, 53-56.
27. W. Pan, W. A. Banks and A. J. Kastin, *J Neuroimmunol*, 1997, **76**, 105-111.
28. V. Bartanusz, D. Jezova, B. Alajajian and M. Digicaylioglu, *Ann Neurol*, 2011, **70**, 194-206.
29. J. L. Shirley, Y. P. de Jong, C. Terhorst and R. W. Herzog, *Mol Ther*, 2020, **28**, 709-722.
30. H. M. Gebril, A. Aryasomayajula, M. R. N. de Lima, K. E. Uhrich and P. V. Moghe, *Translational Neurodegeneration*, 2024, **13**, 2.
31. K. Emmerich, D. T. White, S. P. Kambhampati, G. L. Casado, T.-M. Fu, Z. Chunawala, A. Sahoo, S. Nimmagadda, N. Krishnan, M. T. Saxena, S. L. Walker, E. Betzig, R. M. Kannan and J. S. Mumm, *Communications Biology*, 2023, **6**, 534.
32. G. Zhong, H. Long, T. Zhou, Y. Liu, J. Zhao, J. Han, X. Yang, Y. Yu, F. Chen and S. Shi, *Biomaterials*, 2022, **288**, 121690.
33. M. Battaglini, A. Marino, M. Montorsi, A. Carmignani, M. C. Ceccarelli and G. Ciofani, *Adv Healthc Mater*, 2024, **13**, e2304180.
34. L. C. Schmued and J. H. Fallon, *Brain Res*, 1986, **377**, 147-154.
35. H. T. Chang, H. Kuo, J. A. Whittaker and N. G. Cooper, *J Neurosci Methods*, 1990, **35**, 31-37.
36. L. Novikova, L. Novikov and J. O. Kellerth, *J Neurosci Methods*, 1997, **74**, 9-15.
37. S. E. Mondello, S. C. Jefferson, W. A. O'Steen and D. R. Howland, *J Neurosci Methods*, 2016, **270**, 85-91.
38. M. Bentivoglio, H. G. Kuypers, C. E. Catsman-Berrevoets, H. Loewe and O. Dann, *Neurosci Lett*, 1980, **18**, 25-30.
39. A. Rosina, *Neurosci Lett*, 1982, **33**, 217-221.
40. F. Condé, *J Neurosci Methods*, 1987, **21**, 31-43.
41. F. J. Richmond, R. Gladdy, J. L. Creasy, S. Kitamura, E. Smits and D. B. Thomson, *J Neurosci Methods*, 1994, **53**, 35-46.
42. C. B. Mantilla, W. Z. Zhan and G. C. Sieck, *J Neurosci Methods*, 2009, **182**, 244-249.
43. Y. B. Seven, A. K. Simon, E. Sajjadi, A. Zwick, I. Satriotomo and G. S. Mitchell, *Exp Neurol*, 2020, **323**, 113067.
44. C. R. Gerfen, D. D. O'Leary and W. M. Cowan, *Exp Brain Res*, 1982, **48**, 443-448.
45. P. J. Harrison, H. Hultborn, E. Jankowska, R. Katz, B. Storai and D. Zytnicki, *Neurosci Lett*, 1984, **45**, 15-19.
46. E. Jankowska, *Brain Res*, 1985, **341**, 403-408.
47. H. G. Goshgarian and J. L. Buttry, *J Neurosci Methods*, 2014, **222**, 156-164.
48. J. P. Card, L. Rinaman, J. S. Schwaber, R. R. Miselis, M. E. Whealy, A. K. Robbins and L. W. Enquist, *J Neurosci*, 1990, **10**, 1974-1994.
49. S. Chen, M. Yang, R. R. Miselis and G. Aston-Jones, *Brain Res*, 1999, **838**, 171-183.

View Article Online
DOI: 10.1039/D5NR02670A

50. Z. Boldogköi, A. Reichart, I. E. Tóth, A. Sik, F. Erdélyi, I. Medveczky, C. Llorens-Cortes, M. Palkovits and Z. Lenkei, *Brain Res Mol Brain Res*, 2002, **109**, 105-118.
51. A. E. Granstedt, M. L. Szpara, B. Kuhn, S. S. Wang and L. W. Enquist, *PLoS One*, 2009, **4**, e6923.
52. A. E. Granstedt, B. Kuhn, S. S. Wang and L. W. Enquist, *Cold Spring Harb Protoc*, 2010, **2010**, pdb.prot5410.
53. J. P. Card and L. W. Enquist, *Curr Protoc Neurosci*, 2014, **68**, 1.5.1-1.5.39.
54. J. N. Sleigh, G. A. Weir and G. Schiavo, *BMC Res Notes*, 2016, **9**, 82.
55. Y. B. Seven, R. R. Perim, O. R. Hobson, A. K. Simon, A. Tadjalli and G. S. Mitchell, *J Physiol*, 2018, **596**, 1501-1512.
56. Y. B. Seven, N. L. Nichols, M. N. Kelly, O. R. Hobson, I. Satriotomo and G. S. Mitchell, *Exp Neurol*, 2018, **299**, 148-156.
57. L. L. Allen, N. L. Nichols, Z. A. Asa, A. T. Emery, M. C. Ciesla, J. V. Santiago, A. E. Holland, G. S. Mitchell and E. J. Gonzalez-Rothi, *Exp Neurol*, 2021, **346**, 113832.
58. M. C. Ciesla, Y. B. Seven, L. L. Allen, K. N. Smith, Z. A. Asa, A. K. Simon, A. E. Holland, J. V. Santiago, K. Stefan, A. Ross, E. J. Gonzalez-Rothi and G. S. Mitchell, *Exp Neurol*, 2021, **338**, 113609.
59. M. C. Ciesla, Y. B. Seven, L. L. Allen, K. N. Smith, E. J. Gonzalez-Rothi and G. S. Mitchell, *Exp Neurol*, 2022, **347**, 113903.
60. Y. B. Seven, L. L. Allen, M. C. Ciesla, K. N. Smith, A. Zwick, A. K. Simon, A. E. Holland, J. V. Santiago, K. Stefan, A. Ross, E. J. Gonzalez-Rothi and G. S. Mitchell, *Neuroscience*, 2022, **506**, 38-50.
61. F. J. Golder, D. D. Fuller, M. R. Lovett-Barr, S. Vinit, D. K. Resnick and G. S. Mitchell, *Exp Neurol*, 2011, **231**, 97-103.
62. S. Alvarez-Argote, H. M. Gransee, J. C. Mora, J. M. Stowe, A. J. Jorgenson, G. C. Sieck and C. B. Mantilla, *J Neurotrauma*, 2016, **33**, 500-509.
63. S. Rana, G. C. Sieck and C. B. Mantilla, *J Neurophysiol*, 2017, **117**, 545-555.
64. P. M. Warren, C. Campanaro, F. J. Jacono and W. J. Alilain, *Exp Neurol*, 2018, **306**, 122-131.

View Article Online
DOI: 10.1039/D5NR02670A

UF UNIVERSITY of FLORIDA

College of Veterinary Medicine
Department of Physiological Sciences

1333 Center Drive
PO Box 100144
Gainesville, FL 32610
PH 352-294-4010

March 23rd, 2025

Dr. Quan Li

Re: Submission of manuscript to the *Nanoscale* Journal

Dear Drs. Guldi and Zhang,

The data that support the findings of this study will be made available from the corresponding author, upon reasonable request; starting 1 year after the online publication due to patenting process.

Thank you for your understanding.

Sincerely,

Yasin B. Seven
Assistant Professor
Physiological Sciences
yasinbseven@ufl.edu